Coexistence of superconductivity and charge-density-wave in van der Waals layered material $NbTe_4$

Panyin Li(李潘胤)[1,2,†], Zheng Yin(尹铮)[1,2,†], Dong Li(李栋)[1,2], Chen Ma(马晨)[1,2], Huiru Liu(刘慧如)[1,2,4], Zhe Ying(应哲)[1,2], Jing Teng(滕静)[1,2,4], Yiqi Zhang(章一奇)[1,2], Lan Chen(陈岚)[1,2], Baojie Feng(冯宝杰)[1,2,4], Xiaoyue He(何小月)[4], and Kehui Wu(吴克辉)[3,‡]

[1] *Institute of Physics, Chinese Academy of Sciences, Beijing* 100190, *China*
[2] *School of Physical Sciences, University of Chinese Academy of Sciences, Beijing* 100190, *China*
[3] *Tsientang Institute for Advanced Study, Zhejiang* 310024, *China*
[4] *Songshan Lake Materials Laboratory, Dongguan, Guangdong* 523808, *China*

(Received 10 December 2025; revised manuscript received 25 December 2025; accepted manuscript online 30 December 2025)

Charge density wave (CDW) and superconductivity (SC) have been captivating topics for decades in the field of condensed matter physics, arising from their interplay and correlations with other interesting quantum states. Domain walls in CDW, superconductors, and other ordered systems play an important role in phase transitions and exotic electronic behaviors. Here, we find ambient-pressure superconductivity in the recently reported CDW material $NbTe_4$ by both transport measurements and scanning tunneling spectroscopy. Moreover, using atomically resolved scanning tunneling microscopy, we find that the CDW domain walls of superconducting $NbTe_4$ host unidirectionality, exhibiting anisotropic interactions with the CDW order, specified by Q_{CDW} vectors of the 2×3 bidirectional CDW. This atomic-scale correlation provides insight into the physics of domain walls in condensed matter systems and establishes a possible Q-vector-dependent defect engineering paradigm.

Keywords: charge density wave, superconductivity, coexistence, domain wall, scanning tunneling microscopy

PACS: 74.70.–b, 73.20.Mf, 68.35.B–, 68.37.Ef

DOI: 10.1088/1674-1056/ae31de **CSTR:** 32038.14.CPB.ae31de

CPB Online In Press

Charge density wave (CDW), periodic modulations of electronic charge and lattice structure, represents a fundamental class of collective quantum states in condensed matter physics. Their correlations with superconductivity and other emergent phenomena, such as magnetism and topology, have been subjects of intense research for a long time, revealing profound insights into electron correlations and symmetry breaking.[1–6] Within CDW systems and other ordered states, domain walls play a crucial role. They can significantly influence macroscopic material properties, such as phase transitions,[7–11] electronic transport behaviors,[12–14] and exotic localized states distinct from the bulk.[15–21] In conventional understanding, CDW domain walls are essentially isotropic defects.[9,15] Similar to phase-slip line defects or dislocations, they disrupt the long-range CDW order in a largely directionally independent manner.[22,23] This isotropy stems from the symmetric nature of the order parameter disruption at the wall, irrespective of the specific Q-vectors defining the CDW.

Here, we study the recently reported CDW material $NbTe_4$. As a layered material, $NbTe_4$ hosts a bidirectional 2×3 CDW state (Figs. 1 and 2). By both transport measurements and scanning tunneling spectroscopy, we find that $NbTe_4$ is an interesting CDW superconductor with the superconducting transition temperature around 0.5 K. Moreover, we find unidirectional CDW domain walls on the surface of $NbTe_4$. These domain walls locally transform the bidirectional CDW order into a unidirectional CDW state. The unidirectional orientation is intrinsically governed by the specific Q^{CDW} vectors they interact with. This Q-vector-dependent behavior is in stark contrast to the isotropic nature of conventional CDW defects.

The crystal structure of $NbTe_4$ belongs to space group $P4/mcc$.[24,25] As shown in the schematic structure model in Figs. 1(a) and 1(b), $NbTe_4$ has an intriguing quasi-one-dimensional tubular structure.[24–29] Each quasi-one-dimensional tube consists of Nb atoms located at the axial line and Te atoms surrounding the Nb atoms. The c-axis is along the direction of the quasi-one-dimensional chains, with a lattice constant $c = 0.683$ nm, whereas the lattice constants a and b are both 0.649 nm.[24,26,27] Previous pioneering studies indicate a transition from incommensurate CDW to commensurate 2×3 ordered CDW when lowering temperature below 50 K.[30] However, more experimental evidence is needed to confirm these results since they contradict our experimental results from variable-temperature low-energy electron diffraction (LEED) and scanning tunneling microscopy

[†]These authors contributed equally to this work.
[‡]Corresponding author. E-mail: khwu@tias.ac.cn

© 2026 Chinese Physical Society and IOP Publishing Ltd. All rights, including for text and data mining, AI training, and similar technologies, are reserved.

(STM) experiments. Recently, a commensurate 2×3 CDW order has been observed by STM on a cleaved $NbTe_4$ surface at 1.7 K.[24] In addition, abundant microscopic domain walls are observed along with the 2×3 CDW domains, thus breaking the long-range order of the surface. However, more atomic-scale details are still needed to confirm the CDW order as well as to study domain wall structures since it contradicts our high-resolution STM experiments.

In our experiments, the single crystal $NbTe_4$ was grown by chemical vapor transport method with 99.999% purity. Over 10 samples were cleaved at 77 K in our ultrahigh-vacuum (UHV) chamber with base pressure of 2×10^{-10} mbar, exposing its (010) surface, and then *in-situ* transferred into STM. STM/S measurements were performed in a commercial Unisoku USM1600 STM system for measurements below 4.2 K, and a commercial Infinity STM from Scienta Omicron for measurements at higher temperatures. Our scanning tunneling spectroscopy (STS) measurements were taken by using standard lock-in techniques. The STM tips are chemically etched tungsten tips and Pt/Ir tips. All STM and fast Fourier transform (FFT) images were edited by using WSxM software. The LEED experiments were performed on a commercial SPECS ErLEED 1000-A instrument. Samples were cleaved in the LEED chamber with base pressure of 1×10^{-10} mbar and then the LEED experiments were performed *in-situ* in the same chamber. The low-temperature electron transport experiments were performed by using the conventional four-point probe resistivity measurement method on $NbTe_4$ thin flakes (100 nm thick) so as to measure the bulk superconductivity.

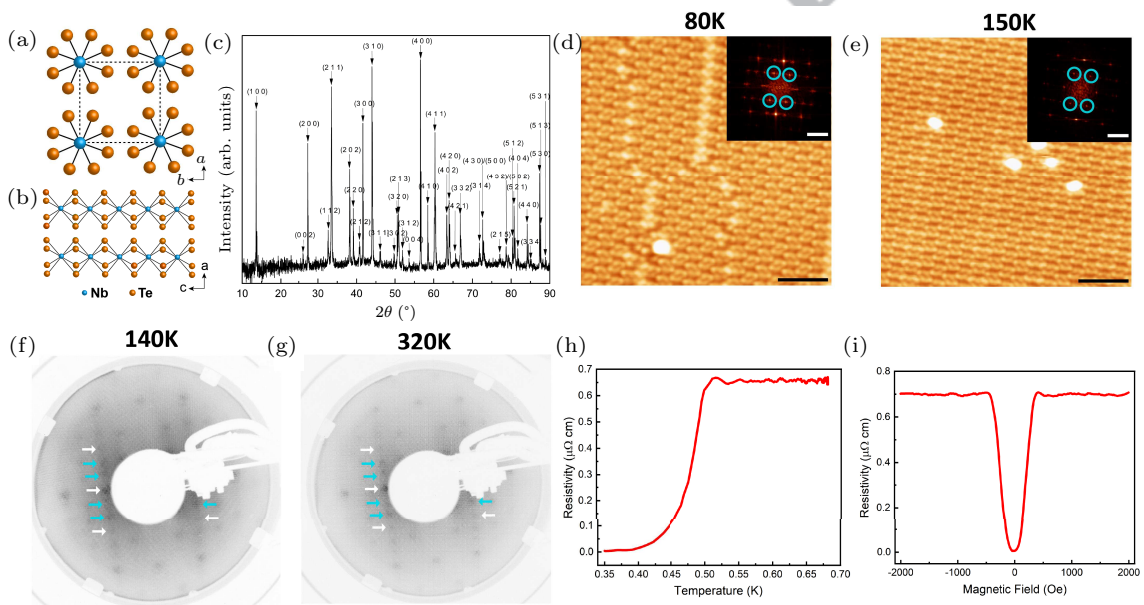


Fig. 1. (a) and (b) Side and top views of the crystal structure of $NbTe_4$, respectively. (c) X-ray diffraction of powder $NbTe_4$. The result confirms the crystal structure of $NbTe_4$ with the $P4/mcc$ space group. (d) and (e) STM images measured at 80 K and 150 K, respectively, with sample bias $V_s = -100$ mV and tunneling current $I = 30$ pA. The scale bar is 4 nm. The FFT (insets) in both images shows the 2×3 CDW points marked by cyan circles. Scale bar: 1.2 nm^{-1}. (f) and (g) LEED patterns of $NbTe_4$ at 140 K and 320 K, respectively. The white arrows indicate 1×1 Bragg spots, and the cyan arrows indicate the 2×3 CDW spots. The slightly blurred LEED spots are due to the small terraces and dense steps formed during the cleaving, leading to large-scale surface roughness. (h) and (i) Electron transport experiments on $NbTe_4$. The insufficient steepness of the ρ–T curve at T_c may be attributed to either defects introduced during the exfoliation of the $NbTe_4$ thin flake sample or the temperature approaching the instrument's cryogenic limit (0.35 K). The magnetic field was applied perpendicular to the a–c plane.

First, we examined the crystal structure of $NbTe_4$ by the x-ray diffraction (XRD) spectrum of powders scratched from a single crystal $NbTe_4$. The result confirms our sample to be $NbTe_4$ with space group $P4/mcc$ (Fig. 1(c)). Figures 1(d) and 1(e) are STM images taken on the $NbTe_4$ surface at 80 K and 150 K, respectively. Both images show the 2×3 bidirectional CDW order that is consistent with the STM image taken at 4.2 K (Fig. 2(a)). Besides, the LEED patterns taken at 140 K and 320 K (Figs. 1(f) and 1(g)) both exhibit 2×3 CDW spots, consistent with theoretically simulated patterns (see Supplementary Fig. S1) and STM images. Hence, our STM and LEED experiments suggest that $NbTe_4$ has a 2×3 CDW order up to 320 K. This transition temperature above room temperature is higher than those of most CDW materials. Here we have to point out that Fig. 1(e) is unfortunately a multi-tip STM image (similar to the multi-tip STM images in Ref. [24]) where there is no evident domain wall. However, it does not affect the demonstration of CDW order in the STM image since the 2×3 points in the FFT (inset of Fig. 1(e)) are present (with weaker magnitude compared to the FFT of Fig. 1(d)). Finally, we performed low-temperature electric transport experiments and discovered the superconductivity in $NbTe_4$ under ambient pressure. The critical temperature T_c is 0.5 K (defined as the onset temperature) (Fig. 1(h)), and the critical field un-

der 0.35 K is 400 G (Fig. 1(i)). Superconductivity at ambient pressure in $NbTe_4$ had never been observed before, since prior studies only measured down to 1.7 K.[24] Importantly, here we discover that the 2×3 bidirectional CDW order can coexist with superconductivity (SC) at ultra-low temperature (0.17 K).

We take STS experiments to detect the CDW and SC states of $NbTe_4$ in more detail. The STM image of the $NbTe_4$ (010) surface taken at 4.2 K shown in Fig. 2(a) reveals the bidirectional CDW order, featuring interlocked Te trimer pairs as illustrated in Fig. 2(c). The green dots represent the top layer Te atoms, which is in agreement with the STM image. One can clearly see the slight Te trimerization caused by CDW formation as guided by the red lines in Fig. 2(b). The original STM image without CDW distortion would be just zigzag chains along the *c*-axis with no Te trimers. Moreover, in contrast to previous work showing non-centrosymmetric Te trimer pairs (which act as the basis of their theoretical explanation of the CDW formation mechanism),[24] our high-resolution STM studies unambiguously show that the charge distribution within the interlocked Te trimer pair is centrosymmetric based on STM experiments of more than 5 cleaved $NbTe_4$ samples (see Supplementary Figs. S2 and S3). Figure 2(d) is the fast Fourier transform (FFT) image of Fig. 2(a), clearly showing the bidirectional CDW wavevectors, marked by Q_1^{CDW} and Q_2^{CDW}, and the Bragg points representing the original 1×1 lattice structure.

For Peierls-type CDW, one major characteristic is the reversed density of states (DOS) distribution in STS maps at the two edges of the CDW gap,[2,3,15,32–35] as the opening of the CDW gap is accompanied by the charge redistribution within the unit cell. Unfortunately, such deterministic data was not achieved in previous STM studies. Here we conducted STS experiments on the $NbTe_4$ (010) surface, as shown in Figs. 2(e), 2(f), and 2(g). The typical dI/dV curve in Fig. 2(e) exhibits a soft gap with non-zero DOS at the Fermi level,[33,35,36] and the CDW gap within edges is $2\Delta = 60$ meV. Besides, the dI/dV maps taken at opposite edges of the CDW gap shown in Figs. 2(f) and 2(g) demonstrate intensity reversal. The symmetric CDW gap located at the Fermi level together with the dI/dV intensity reversal unambiguously indicate a Peierls-type CDW order in $NbTe_4$.

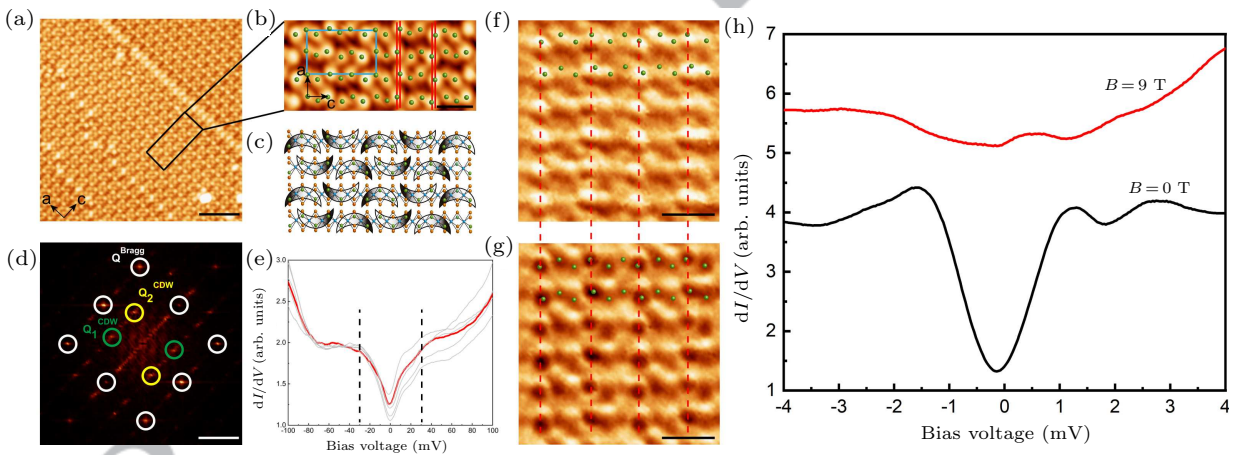


Fig. 2. STM/S characterization on $NbTe_4$. (a) Constant-current STM image of $NbTe_4$, measured with $V_s = -100$ mV and $I = 100$ pA. Scale bar: 4 nm. (b) Cropped image of (a) marked by the black rectangle. The Bragg lattice vectors and the unit cell of the 2×3 CDW superstructure are marked by black arrows and a blue rectangle, respectively. Scale bar: 1 nm. (c) Schematic model of (b). The Te trimers that consist of three top-layer Te atoms marked by green dots are represented by black and white gradient crescents, where the darker the color, the greater the intensity. (d) The FFT image of (a). The 1×1 spots are marked by white circles and two CDW wavevectors are marked by the green and yellow circles, respectively. Scale bar: 1.2 nm^{-1}. (e) dI/dV curve taken on $NbTe_4$. The red curve shows a soft gap of CDW order, where the edges of the gap (± 30 meV) are defined by turning points of the curve and marked by black dashed lines. Gray curves are repetitive dI/dV spectroscopy, which are in good agreement with the red curve. (f) and (g) dI/dV maps taken on $NbTe_4$ at opposite edges of the CDW gap: -30 mV and 30 mV, respectively. The dI/dV maps at -30 mV and 30 mV exhibit charge accumulation and depletion regions, respectively. The red dashed lines represent the same spatial positions. Scale bar: 1 nm. The STS measurements in panels (e), (f), and (g) were taken by using standard lock-in techniques with a bias modulation of 5 mV at 983 Hz. (h) dI/dV spectroscopy on $NbTe_4$ at a modulation frequency of 987 Hz and a modulation bias of 500 μV.

Finally, we took dI/dV under 0.17 K within the energy range of -4 mV to 4 mV and obtained the SC-shape gap when the external magnetic field is 0 T (Fig. 2(h)). Then we took dI/dV with the external magnetic field $B = 9$ T under the same temperature, and the SC-shape gap disappeared, which confirms that the observed gap is a SC gap. At the same time, we examined the atomic-scale STM images of $NbTe_4$ in the superconducting state (see Supplementary Fig. S3). It clearly shows the 2×3 bidirectional CDW order and the centrosymmetric charge distribution although the image is distorted. Therefore, the bidirectional CDW order and SC state coexist in $NbTe_4$. Previous studies have reported pressure-induced SC in $NbTe_4$ with $T_c = 2.2$ K under 69 GPa.[31] They found that the CDW order is greatly suppressed under high pressure so that the SC state can be released due to the competing nature between CDW and SC in $NbTe_4$. The coexistence of the

CPB In-Press

superconducting phase and CDW is not contradictory to the competitive relationship between the two. In fact, many classic materials exhibit this behavior, such as 2H-$NbSe_2$.[37,38] So $NbTe_4$ may be one of them.

Another important feature in the STM images of the $NbTe_4$ surface is the abundant domain wall structures, as shown in the large-area image (see Supplementary Fig. S4). The formation of CDW domain walls breaks the long-range order of the surface, resulting in separated CDW domains and domain walls between them. We observed in total four different kinds of CDW domain walls (α_1, α_2, β_1, β_2) as illustrated in Fig. 3. Interestingly, all four domain walls are along the a axis. As seen in Figs. 3(b) and 3(c), the α_1 domain wall consists of alternating Te dimers with different orientations (one upper-leftward stroke and one upper-rightward stroke). The α_2 domain wall has exactly the same structure (Figs. 3(d) and 3(e)) but a different alternating order of Te dimers as compared with α_1. The β_1 and β_2 domain walls have distinct structures. As shown in Figs. 3(g) and 3(h), the β_1 domain wall only consists of upper-rightward-stroke Te dimers that distribute one dimer on every other zigzag Te chain. The β_2 domain wall has the same structure as β_1, but with only upper-leftward-stroke Te dimers. For stability, the number density of α domain walls is much lower than that of β domain walls (see Supplementary Fig. S4). Moreover, we discovered that the α domain walls and β domain walls can transform into each other under the influence of tip-induced electric fields at $V_s = 1$ V. But they are stable when scanning at $V_s = 100$ mV. We have not yet identified systematic rules governing the transformation between the two. However, in most cases, α domain walls transform into β domain walls when scanning at $V_s = 1$ V, after which the β domain walls gradually shorten until they eventually vanish. These two points indicate that the β domain walls are energetically more stable than the α domain walls.

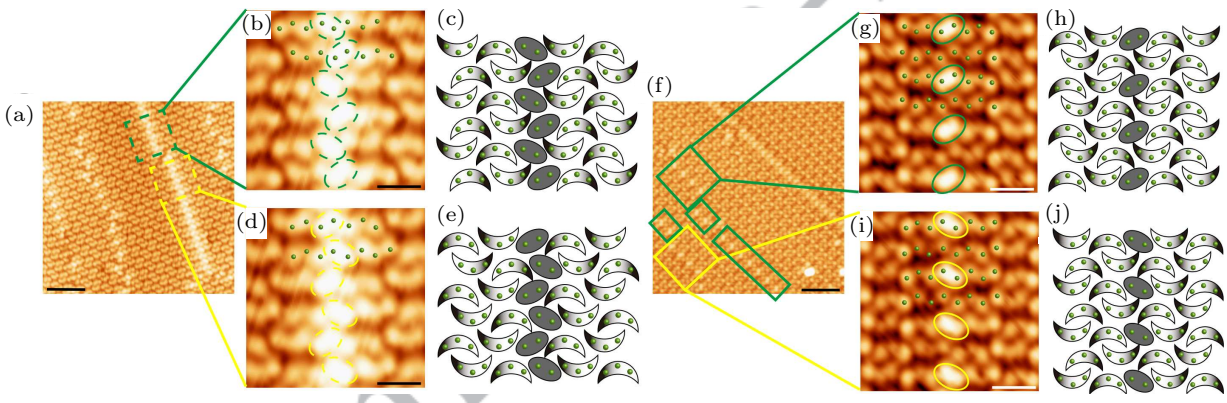


Fig. 3. Atomic-scale STM images showing the structures of α and β domain walls. (a) Constant-current STM image of $NbTe_4$. The regions marked by green and yellow dashed rectangles represent the α_1 and α_2 domain walls. The image was taken at $V_s = 100$ mV and $I = 100$ pA. Scale bar: 4 nm. (b) and (c) Cropped STM image and schematic model of α_1 domain wall. The green dots represent the top-layer Te atoms. The green dashed ellipses represent the Te dimers that form the α_1 domain wall. Scale bar: 1 nm. (d) and (e) Cropped STM image and schematic model of α_2 domain wall. The yellow dashed ellipses represent the Te dimers that form the α_2 domain wall. Scale bar: 1 nm. (f) Constant-current STM image of another region of $NbTe_4$. The regions marked by green and yellow rectangles represent the β_1 and β_2 domain walls. The image was taken at $V_s = -100$ mV and $I = 100$ pA. Scale bar: 4 nm. (g) and (h) STM image and schematic model of β_1 domain wall. The green ellipses represent the Te dimers that form the β_1 domain wall. Scale bar: 1 nm. (i) and (j) STM image and schematic model of β_2 domain wall. The yellow ellipses represent the Te dimers that form the β_2 domain wall. Scale bar: 1 nm.

We are interested in digging deeper into how these domain walls disrupt the CDW order. The knowledge of the exact nature of the directionality of each domain wall type is significant to understanding the physical nature of CDW. As we all know, domain walls disrupt long-range order and break it into small domains. Generally, such disruption is directionally non-selective. Domains on either side of a boundary may exhibit different orders (e.g., two unidirectional CDWs with different orientations). However, if we consider the local region that includes the domain wall itself, the boundary possesses no inherent directionality — it merely serves to break long-range order.

In the case of $NbTe_4$, we find that there exists a type of CDW domain boundary that, within its local region, directionally disrupts the CDW order, while the CDW domains on both sides remain identical. This indicates that such a CDW domain wall itself can be regarded, in a sense, as a unidirectional CDW. It may profoundly affect the electronic structure and transport properties of $NbTe_4$, which will be a key focus of our future research. First, we take a series of FFT images from STM images consisting of β_1 and β_2 domain walls with different lengths. The length of β domain walls is defined by the Te dimers contained as illustrated by the green and yellow ellipses. In Figs. 4(a) and 4(b), we take β_1 and β_2 domain walls containing four Te dimers as examples. The FFT image (Fig. 4(c)) clearly shows that the FFT amplitude of the CDW peak along Q_2^{CDW} is dominantly greater than the CDW peak along Q_1^{CDW}, which means β_1 domain wall only breaks CDW order along Q_1^{CDW}. Therefore, the region in Fig. 4(a) transits from bidirectional CDW to unidirectional CDW due

to the existence of β_1 domain wall. Similarly, the region in Fig. 4(b) transits from bidirectional CDW to unidirectional CDW along Q_1^{CDW}. Therefore, β_1 and β_2 domain walls are unidirectional domain walls. We examine the amplitude of CDW peaks along different Q^{CDW} to quantify the unidirectionality of β domain walls. Figures 4(e) and 4(f) are the line profiles along the path marked by white arrows in Figs. 4(c) and 4(d), respectively. In Fig. 4, green, yellow, and white circles represent Q_1^{CDW}, Q_2^{CDW} and Q^{Bragg}, respectively, where $\boldsymbol{Q}^{\mathrm{Bragg}} = (\frac{1}{a}, 0)$, $\boldsymbol{Q}^{\mathrm{CDW}} = (\frac{1}{2a}, \frac{1}{3c})$. So, the center of peaks in all line profile diagrams is $|\boldsymbol{Q}^{\mathrm{CDW}}/||\boldsymbol{Q}^{\mathrm{Bragg}}| = 0.58$. Then we calculate the areas of CDW peaks marked by the blue rectangle regions (where most of the weight can be contained, and the width of the CDW peak is $\sigma = 0.33 \times Q^{\mathrm{Bragg}} = 0.50\ \mathrm{nm}^{-1}$) in all line profiles (Fig. 4 and Supplementary Fig. S5) and obtain Fig. 4(g) which shows the relationship between the proportion of areas of CDW peaks along two different Q^{CDW} (defined as $\frac{\text{areas with higher value}}{\text{areas with lower value}}$) and the length of domain walls. From Fig. 4(g), we can see that β_1 and β_2 domain walls maintain unidirectionality no matter what the length of domain wall is. And for both β_1 and β_2 domain walls, the one that has four Te dimers possesses the largest unidirectionality.

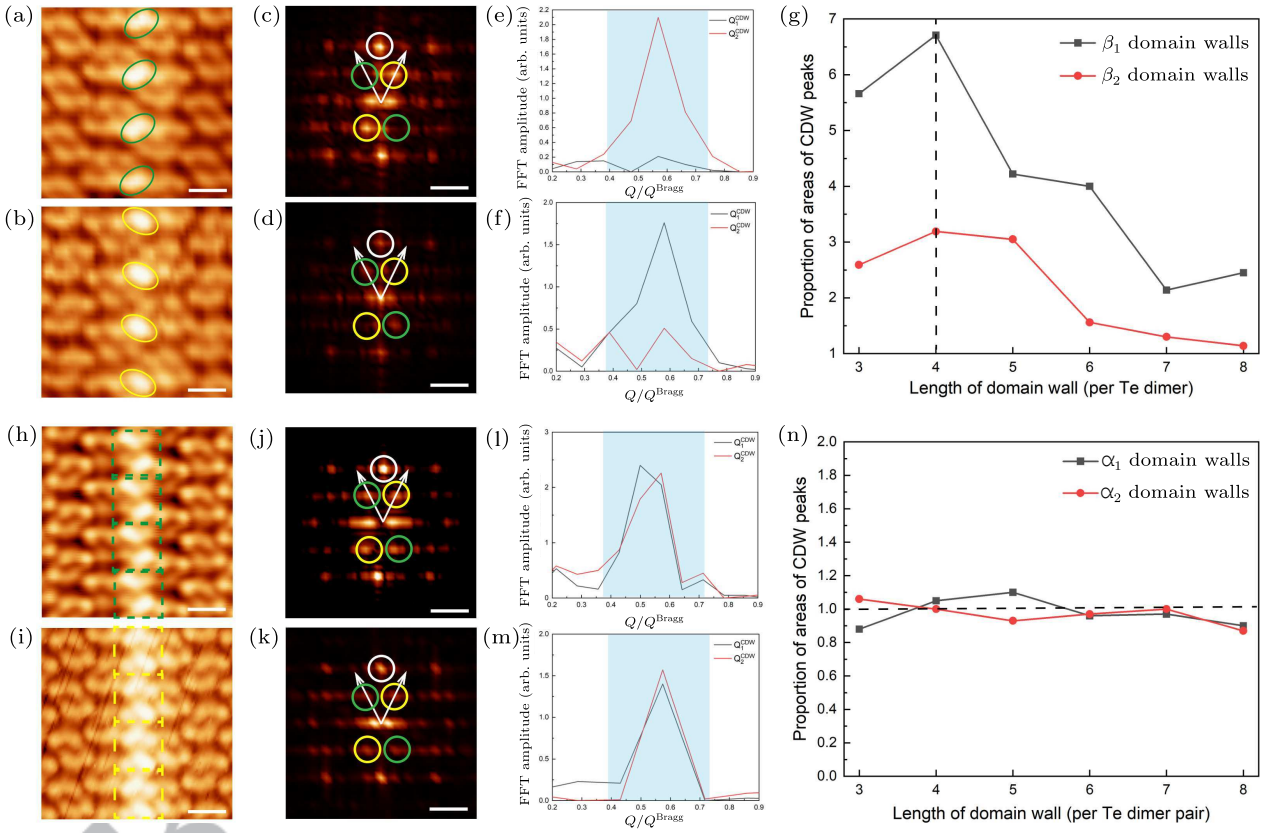


Fig. 4. Analysis of unidirectionality in α and β domain walls. (a) and (b) Cropped STM images of $NbTe_4$ with β_1 and β_2 domain walls, respectively. The image was taken at $V_s = 100$ mV and $I = 100$ pA. Scale bar: 1 nm. (c) and (d) FFT images of (a) and (b), respectively. Scale bar: 1.2 nm^{-1}. (e) and (f) Line profiles along the paths indicated by white arrows in (c) and (d). The black and red curves represent the line profiles along Q_1^{CDW} and Q_2^{CDW}, respectively. (h) and (i) Cropped STM images of $NbTe_4$ with α_1 and α_2 domain walls, respectively. The image was taken at $V_s = 100$ mV and $I = 100$ pA. The Te dimer pairs are marked by green and yellow dashed rectangles, respectively. Scale bar: 1 nm. (j) and (k) FFT images of (h) and (i), respectively. Scale bar: 1.2 nm^{-1}. (l) and (m) Line profiles along the paths indicated by white arrows in (j) and (k). (g) and (n) The statistical diagrams showing the relationship between the proportion of areas of CDW peaks and the length of domain walls for β and α domain walls, respectively.

On the other hand, we also performed the FFT and line profile analysis for α_1 and α_2 domain walls. We take α_1 and α_2 domain walls with four Te dimer pairs as examples (Figs. 4(h) and 4(i)). From the FFT images (Figs. 4(j) and 4(k)), we can see that there is no evident difference in CDW peaks Q_1^{CDW} and Q_2^{CDW}. Quantitatively, the areas of CDW peaks are equal for Q_1^{CDW} and Q_2^{CDW} (Figs. 4(l), 4(m), 4(n) and Supplementary Fig. S6) no matter what the length of the domain wall is. Hence, α_1 and α_2 domain walls are not unidirectional. They do not locally break the bidirectional CDW order.

From another perspective, we also applied the known two-dimensional (2D) lock-in technique as a complementary approach to further verify the unidirectionality of α and β domain walls (see more details in Supplementary information).

In summary, we have experimentally discovered the coexistence of bidirectional CDW order and ambient-pressure superconductivity in $NbTe_4$. Moreover, we find that β-type CDW domain walls anisotropically disrupt the CDW order and locally transform bidirectional CDW order into unidirectional

CDW order. Our work raises important questions about the relationship between superconductivity and the unidirectional behavior of domain walls in charge density waves. Understanding the origin of this phenomenon could provide insights into other ordered systems with various domain walls.[12,22,39]

Acknowledgment

The authors acknowledge the financial support from Hangzhou Tsientang Education Foundation.

References

[1] Fradkin E, Kivelson S A and Tranquada J M 2015 *Rev. Mod. Phys.* **87** 457
[2] Monceau P 2012 *Adv. Phys.* **61** 325
[3] Gruner G 1994 *Density Waves in Solids* (1st edn.) (Boca Raton: CRC Press)
[4] Cao Z Y, Chen H, Qian G J, Shi Y H, Qi Q, Han X H, Yang H T and Gao H J 2025 *Chin. Phys. Lett.* **42** 100702
[5] Lin Y H, Dong J W, Fu R, Wu X, Wang Z and Zhou S 2025 *Chin. Phys. Lett.* **42** 080709
[6] Liu X, Lai J, Zhan J, Yu T, Shi W, Liu P, Chen X Q, and Sun Y 2025 *Chin. Phys. Lett.* **42** 037302
[7] Gao P, Britson J, Jokisaari J R, Nelson C T, Baek S H, Wang Y, Eom C B, Chen L Q and Pan X 2013 *Nat. Commun.* **4** 2791
[8] Lee S, Kim E, Bang J, Park J, Kim C, Wulferding D and Cho D 2023 *Nano Lett.* **23** 11219
[9] Park J W, Cho G Y, Lee J and Yeom H W 2019 *Nat. Commun.* **10** 4038
[10] Yan S, Iaia D, Morosan E, Fradkin E, Abbamonte P and Madhavan V 2017 *Phys. Rev. Lett.* **118** 106405
[11] Zong A, Shen X Z, Kogar A, Ye L, Marks C, Chowdhury D, Rohwer T, Freelon B, Weathersby S, Li R K, Yang J, Checkelsky J, Wang X J and Gedik N 2018 *Sci. Adv.* **4** eaau5501
[12] Catalan G, Seidel J, Ramesh R and Scott J F 2012 *Rev. Mod. Phys.* **84** 119
[13] Lee S, Collini J, Sun S X L, Mitrano M, Guo X, Eckberg C, Paglione J, Fradkin E and Abbamonte P 2021 *Phys. Rev. Lett.* **127** 027602
[14] Vaskivskyi I, Mihailovic I A, Brazovskii S, Gospodaric J, Mertelj T, Svetin D, Sutar P and Mihailovic D 2016 *Nat. Commun.* **7** 11442
[15] Barja S, Wickenburg S, Liu Z F, Zhang Y, Ryu H, Ugeda M M, Hussain Z, Shen Z X, Mo S K, Wong E, Salmeron M B, Wang F, Crommie M F, Ogletree D F, Neaton J B and Weber-Bargioni A 2016 *Nat. Phys.* **12** 751
[16] Cho D, Gye G, Lee J, Lee S H, Wang L, Cheong S W and Yeom H W 2017 *Nat. Commun.* **8** 392
[17] Ma E Y, Cui Y T, Ueda K, Tang S J, Chen K, Tamura N, Wu P M, Fujioka J, Tokura Y and Shen Z X 2015 *Science* **350** 538
[18] Skolimowski J, Gerasimenko Y and Žitko R 2019 *Phys. Rev. Lett.* **122** 036802
[19] Xia Y, Zhang J, Jin Y, Ho W, Xu H and Xie M 2020 *ACS Nano* **14** 10716
[20] Zhu T C, Ruan W, Wang Y Q, Tsai H Z, Wang S, Zhang C X, Wang T Y, Liou F, Watanabe K, Taniguchi T, Neaton J B, Weber-Bargioni A, Zettl A, Qiu Z Q, Zhang G Y, Wang F, Moore J E and Crommie M F 2022 *Nat. Mater.* **21** 748
[21] Leridon B, Caprara S, Vanacken J, Moshchalkov V V, Vignolle B, Porwal R, Budhani R C, Attanasi A, Grilli M and Lorenzana J 2020 *New J. Phys.* **22** 073025
[22] Lin Z K, Wang Q, Liu Y, Xue H, Zhang B, Chong Y and Jiang J H 2023 *Nat. Rev. Phys.* **5** 483
[23] Kleman M and Friedel J 2008 *Rev. Mod. Phys.* **80** 61
[24] Galvis J A, Fang A, Jiménez-Guerrero D, Rojas-Castillo J, Casas J, Herrera O, Garcia-Castro A C, Bousquet E, Fisher I R, Kapitulnik A and Giraldo-Gallo P 2023 *Phys. Rev. B* **107** 045120
[25] Selte K, Kjekshus A, Petersen C S, Halvarson H and Nilsson L 1964 *Acta Chem. Scand.* **18** 690
[26] Boswell F, Prodan A and Brandon J 1983 *J. Phys. C: Solid State Phys.* **16** 1067
[27] van Smaalen S, Bronsema K and Mahy J 1986 *Struct. Sci.* **42** 43
[28] Prodan A and Boswell F 1987 *Struct. Sci.* **43** 165
[29] Walker M and Morelli R 1988 *Phys. Rev. B* **38** 4836
[30] Eaglesham D J, Bird D, Withers R L and Steeds J W 1985 *J. Phys. C: Solid State Phys.* **18** 1
[31] Yang X J, Zhou Y H, Wang M M, Bai H, Chen X L, An C, Zhou Y, Chen Q, Li Y P, Wang Z, Chen J, Cao C, Li Y K, Zhou Y, Yang Z R and Xu Z A 2018 *Sci. Rep.* **8** 6298
[32] Zhu X, Cao Y, Zhang J, Plummer E and Guo J 2015 *Proc. Natl. Acad. Sci. USA* **112** 2367
[33] Yin J X, Jiang Y X, Teng X, Hossain M S, Mardanya S, Chang T R, Ye Z J, Xu G, Denner M M, Neupert T, Lienhard B, Deng H B, Setty C, Si Q M, Chang G Q, Guguchia Z, Gao B, Shumiya N, Zhang Q, Cochran T A, Multer D, Yi M, Dai P C and Hasan M Z 2022 *Phys. Rev. Lett.* **129** 166401
[34] Rossnagel K 2011 *J. Phys.: Condens. Matter* **23** 213001
[35] Jiang Y X, Yin J X, Denner M M, Shumiya N, Ortiz B R, Xu G, Guguchia Z, He J Y, Hossain M S, Liu X X, Ruff J, Kautzsch L, Zhang S S, Chang G Q, Belopolski I, Zhang Q, Cochran T A, Multer D, Litskevich M, Cheng Z J, Yang X P, Wang Z Q, Thomale R, Neupert T, Wilson S D and Hasan M Z 2021 *Nat. Mater.* **20** 1353
[36] Sun H G, Shao Z B, Luo T C, Gu Q Q, Zhang Z Y, Li S J, Liu L J, Gedeon H, Zhang X, Bian Q, Feng J, Wang J and Pan M H 2020 *New J. Phys.* **22** 083025
[37] Xi X X, Zhao L, Wang Z F, Berger H, Forró L, Shan J and Mak K F 2015 *Nat. Nanotechnol.* **10** 765
[38] Lian C S, Si C and Duan W H 2018 *Nano Lett.* **18** 2924
[39] Meier D and Selbach S M 2022 *Nat. Rev. Mater.* **7** 157

CP Online IOP Press